Available online at www.sciencedirect.com
SCIENCE DIRECT®
Journal of Power Sources 123 (2003) 216–221
JOURNAL OF POWER SOURCES
www.elsevier.com/locate/jpowsour

Anode behaviors of magnesium–antimony intermetallic compound for lithium secondary battery

Hitohiko Honda, Hiroki Sakaguchi, Ichiro Tanaka, Takao Esaka*

Department of Materials Science, Faculty of Engineering, Tottori University, Minami 4-101, Koyama-cho, Tottori 680-8552, Japan

Abstract

Mg_3Sb_2 with a structure of A-type rare earth oxide (hexagonal) was synthesized by mechanical alloying (MA) and evaluated as a negative electrode material for rechargeable lithium batteries. Electrochemical tests demonstrated that the initial charge and discharge capacities of Mg_3Sb_2 were ca. 850 and 600 mA h g^{-1}, respectively. Ex situ XRD of the Mg_3Sb_2 electrodes showed that several lithium-containing compounds such as LiMgSb and Li_3Sb were successively formed during the insertion of lithium into Mg_3Sb_2. As to LiMgSb synthesized by MA-method, the electrode performance was also investigated; it showed an excellent reversibility at the first cycle and a rechargeable capacity of ca. 200 mA h g^{-1} after the fourth cycle. The cycle life performance of LiMgSb electrode was significantly enhanced in comparison with that of Mg_3Sb_2.

Keywords: Lithium battery; Anode material; Mg_3Sb_2; Lithium storage; Intermetallic compound

1. Introduction

Recently, there has been a considerable interest in seeking intermetallic compounds as anode materials of rechargeable lithium batteries, because the materials with higher volumetric and gravimetric capacities have been expected besides the conventional carbon materials [1–30]. However, the electrode reactions of many intermetallic compounds accompany several phase changes, which cause volume expansion and contraction during lithium-insertion and extraction. The large volume changes limit the charge–discharge performances of secondary batteries. Among them, the cycle life performance can be significantly improved in the composite electrodes, such as SnFe/SnFeC [6] and Sn/SnSb [7–9], in which active component to lithium is finely dispersed in the inactive one. In these compounds, the active element reacts with lithium to form lithium alloys, while the inactive plays the role of matrix, which moderates volume expansion of the dispersed active phase during the charge–discharge cycle. As a result, the disintegration of electrode is suppressed and the cyclability is changed for the better.

On the other hand, Kepler et al. [10,11] and Dahn and co-workers [12] have reported a unique lithium-insertion intermetallic electrode consisting of Cu_6Sn_5 [10–13]. The compound could accommodate lithium with relatively small volume change as well as the Mg_2Ge electrode previously reported [14–17]. Cu_6Sn_5 has a defect NiAs-type structure (hexagonal system) in which 20% of the interstitial sites are occupied by copper. On lithiation, at first, Cu_6Sn_5 can topotactically react with lithium to yield Li_2CuSn with a structure closely resembled to Cu_6Sn_5; while the inserted lithium is substituted for copper in Cu_6Sn_5 structure, the other copper and tin atoms stay at their own spatial positions; the reversible gravimetric capacity is ca. 200 mA h g^{-1}, which corresponds to a volumetric capacity of ca. 1360 mA h cm^{-3} based on an average electrode density of 6.8 g cm^{-3}. Although a 59% expansion in volume is accompanied by the phase transition, it is smaller expansion for binary lithium-metal systems, such as Li_xAl, Li_xSb and Li_xSn. As a result, on further charging to lower potentials, a reversible displacement reaction occurs; copper is extruded from Li_2CuSn to produce the copper and lithium–tin alloy composite.

The magnesium–antimony system is crystallographically similar to Cu_6Sn_5/Li_2CuSn. Fig. 1 gives the crystal structures of hexagonal Mg_3Sb_2 with the A-type rare earth oxide structure and cubic LiMgSb with the MgAgAs-type structure, to which the projections along c axis of Mg_3Sb_2 and (1 1 1) direction of LiMgSb are added, respectively. The lithium atoms were sandwiched between layers of antimony and magnesium atoms. The antimony atom maintains its spatial position (a network of antimony atoms) during the reaction of Mg_3Sb_2 with lithium, although some

* Corresponding author. Tel.: +81-857-31-5264; fax: +81-857-31-5264.
E-mail address: esaka@chem.tottori-u.ac.jp (T. Esaka).

0378-7753/$ – see front matter © 2003 Elsevier Science B.V. All rights reserved.
doi:10.1016/S0378-7753(03)00517-2

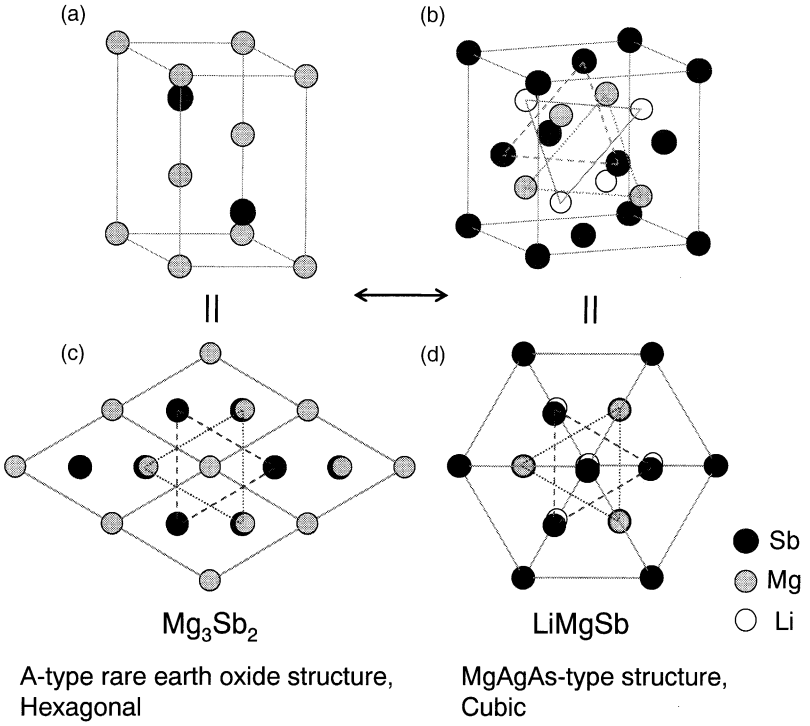

Fig. 1. Schematic drawings of the A-type rare earth oxide structure of (a) hexagonal Mg_3Sb_2, and the MgAgAs-type structure of (b) cubic LiMgSb, and projections along *c*-axis and (1 1 1) direction of the corresponding crystal structures (c), (d).

magnesium atoms are extruded from the LiMgSb lattice. Using the crystal parameters of Mg_3Sb_2 and LiMgSb, the volumetric increase is calculated to be 10% per Sb lattice. If the transition proceeds reversibly, the intermetallic compound may be an attractive alternative to graphite, having the advantage of high volumetric capacity. In the present work, we were going to synthesize Mg_3Sb_2 and LiMgSb by the mechanical alloying (MA) technique, and the electrode performance was investigated on the resultant samples.

2. Experimental

Since magnesium has a high vapor pressure, magnesium-based alloys are difficult to be synthesized with stoichiometric compositions by a metallurgical method. Here, mechanical alloying was considered to be a suitable method. A mixture of elemental magnesium (Wako Pure Chemical Industries, more than 99.0% pure, particle size ca. 300–500 μm) and antimony (Goodfellow Cambridge, more than 99.2% pure, particle size ca. 50 μm) powders was put in a stainless-steel vessel (80 ml) together with five balls (15). The Mg/Sb ratio was 1.5, and the weight ratio of the balls to the sample was about 15:1. The vessel used was sealed with an O-ring to keep an atmosphere of dry argon gas (more than 99.99% pure). The milling was done using a high-energy planetary ball mill (Itoh, LP-4/2) at 300 rpm and at room temperature. In the same manner, LiMgSb was synthesized with magnesium and antimony powders and lithium chip (99.98%, ca. 1 mm square, Mitsui Mining & Smelting) as starting materials.

To identify phases of mechanically alloyed samples, X-ray diffraction (Shimadzu, XRD-6000) was carried out using Ni-filtered Cu Kα radiation at a 2θ scan of $2^\circ\,min^{-1}$. A step-scanning method (2.4 s/0.020°) was applied to estimate lattice constants. The chemical composition and impurities were determined with ICP emission spectroscope (Shimadzu, ICPS-5000). The sample powders obtained were observed by scanning electron microscopy (SEM) in order to know the sample morphology and the particle size. The particle size distribution was measured with Shimadzu SALD-2100 laser diffraction particle size analyzer, in which the suspensions were treated with ultrasound before and during the measurement to break larger suspensoid aggregates down to smaller ones.

The electrochemical properties of the materials were measured with a three-electrode cell, in which both counter and reference electrodes were 1 mm thick lithium-metal sheets (99.98%) supplied by Mitsui Mining & Smelting. An amount of 1 M $LiClO_4$ dissolved in propylene carbonate (PC) (Kishida Chemical) was used as an electrolyte. The test electrodes were fabricated by pressing the Mg_3Sb_2 powder onto a copper mesh (5 mm × 5 mm) under a pressure of 200 kgf cm^{-2}. Neither conductive material nor binder was used for the construction of electrode. The cell performance was evaluated galvanostatically at a current density of 0.4 mA cm^{-2} for both charge and discharge at 30 °C.

Cyclic voltammetric measurements were carried out with the three-electrode cell at the scan rate of 0.1 mV s^{-1}.

To clarify the electrode reaction mechanism, ex situ XRD was done for the Mg_3Sb_2 electrodes obtained by stopping lithium-insertion/extraction at various voltages. In each case, the testing sample was peeled off from the copper mesh and was dried overnight in vacuo.

3. Results and discussion

Fig. 2 shows XRD patterns of the mechanically alloyed products. After 10 h milling, the diffraction pattern corresponded to a hexagonal phase of the JCPDS data with an A-type rare earth oxide structure, although a trace of diffraction peak of antimony was observed. From the ICP measurement, the sample mechanically alloyed for 10 h had a composition of $Mg_3Sb_{2.03}Fe_{0.11}Cr_{0.01}Ni_{0.03}$, which denoted that the sample was prepared almost stoichiometrically, although insignificant contamination was derived from the stainless-steel vessel and balls. The particle size including aggregates distributed over a wide range centered around 10 μm. SEM images of the sample powders were used to estimate a primary particle size, which was ranged 2–3 μm for the sample ball-milled for 10 and 30 h.

Fig. 3 illustrates charge–discharge curves of the Mg_3Sb_2 electrode synthesized by MA technique for 30 h. Although the Mg_3Sb_2 electrode was prepared without any binder and conductive material such as graphite and acetylene black, the first charge (lithium-insertion) capacity was ca. 800 mA h g^{-1}, suggesting Mg_3Sb_2 has a large latent power density as an anode material for lithium batteries. On the other hand, the first discharge (lithium-extraction) capacity was ca. 600 mA h g^{-1}, which was almost the same level as that of the non-graphitizable (hard) carbon electrode. However, it was noteworthy that considering the density of Mg_3Sb_2 (4.0 g cm^{-3}) the volumetric discharge capacity was 2400 mA h cm^{-3}, which was much larger than that of

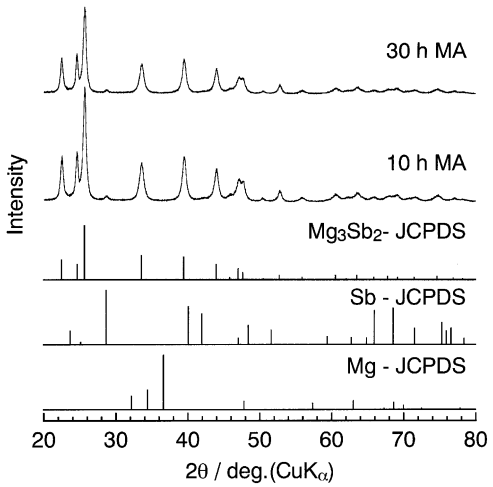

Fig. 2. XRD patterns of the mechanical alloyed Mg–Sb mixture.

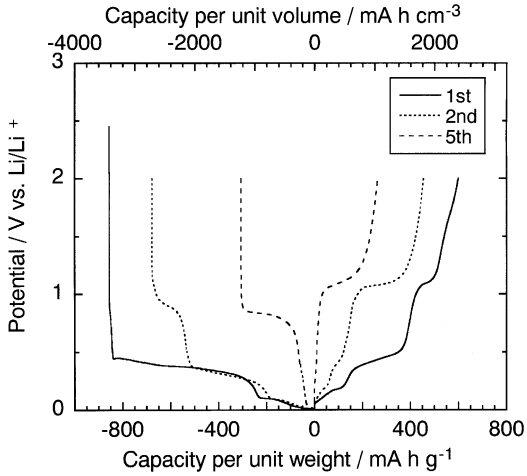

Fig. 3. Charge–discharge curves for the electrode of Mg_3Sb_2 synthesized by mechanical alloying.

the graphite electrode of ca. 800 mA h cm^{-3}. Assuming a reaction mechanism with formation of Li_3Sb by

$$6Li^+ + 6e^- + Mg_3Sb_2 \rightarrow 2Li_3Sb + 3Mg, \quad (1)$$

the density of the fully lithiated sample was calculated using a weighted average of 3Mg and 2Li_3Sb. If one used the resulting value, 3.04 g cm^{-3}, the volumetric capacity was estimated to be about 1820 mA h cm^{-3} for the gravimetric capacity of 600 mA h g^{-1}. At the fifth cycle, however, the capacity of Mg_3Sb_2 electrode was reduced by half. Fig. 3 also shows the change in the potential profiles of the Mg_3Sb_2 electrode in early few cycles. The dominant voltage plateau shifted from 0.4 to 0.8 V for lithium-insertion and from 0.4 to 1.0 V for lithium extraction. As the plateaus showed the co-existence of Mg_3Sb_2 and lithium-containing compounds, the change in the plateaus would suggest that the reaction in the Mg_3Sb_2 electrode varied with charge–discharge cycling. To check phase changes during the electrochemical lithiation, XRD was carried out on the samples obtained at various Li-insertion steps (Fig. 4). The single Mg_3Sb_2 phase before cycling changed to the LiMgSb phase during the initial lithium-insertion process down to 0.2 V, indicating an obvious phase transition as mentioned above (Fig. 1). When the potential reached to 0 V, Li_3Sb was confirmed as a new phase from the precise XRD peak analysis. As for the lithium extraction process up to 1.3 V, the Li 3Sb phase was found to disappear and the LiMgSb phase was restructured.

The cyclic voltammogram of the Mg_3Sb_2 electrode, as shown in Fig. 5, was compared with that of the elemental antimony electrode. For the Mg_3Sb_2 electrode, a large cathodic current peak appeared below 0.5 V in the first reduction half-cycle, but not at the sixth cycle; the profiles were completely different between the first and the sixth cycles. Considering the result of Fig. 5b, however, the peak profile was similar to that of the elemental antimony electrode. These results suggested that the lithium-insertion mechanism of Mg_3Sb_2 was varied with repeating the charge–discharge

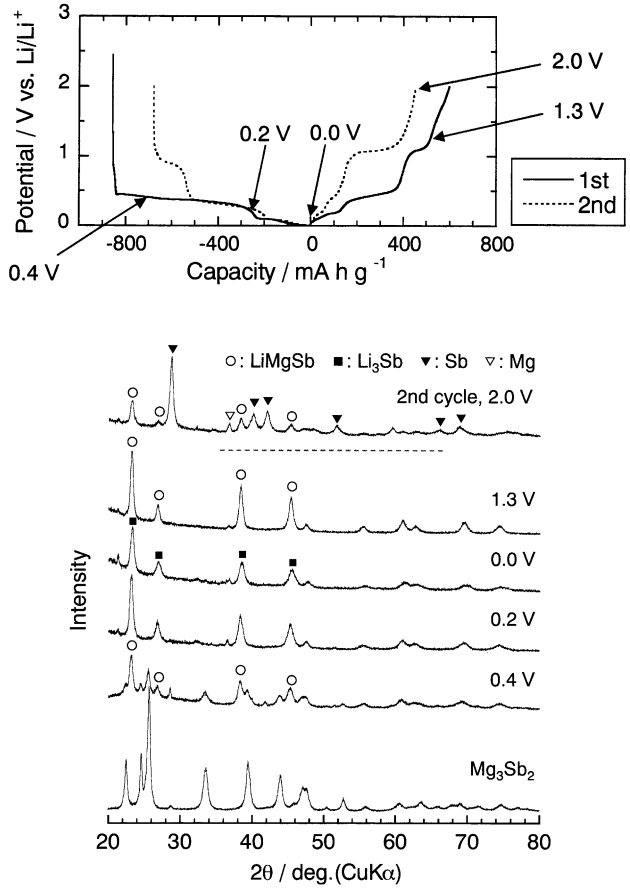

Fig. 4. XRD patterns of Mg_3Sb_2 at various lithiated steps.

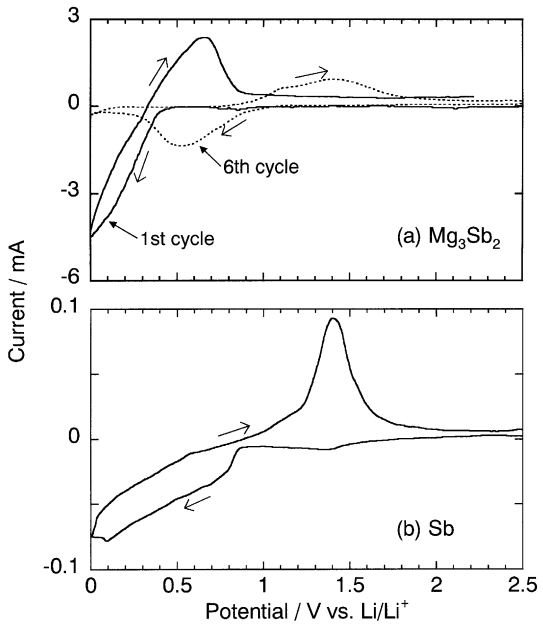

Fig. 5. Cyclic voltammograms ($0.1\,mV\,s^{-1}$) for the electrodes consisting of (a) Mg_3Sb_2 and (b) metallic Sb.

cycle, and based on the formation of Li–Sb alloy. From the ex situ XRD and the cyclic voltammetry for the Mg_3Sb_2 electrodes, the reactions in the Mg_3Sb_2 electrodes during the charge process could be written as:

$$Mg_3Sb_2 + 2Li^+ + 2e^- \rightarrow 2LiMgSb + Mg, \quad (2)$$

$$LiMgSb + 2Li^+ + 2e^- \rightarrow Li_3Sb + Mg. \quad (3)$$

The reversibility of the reaction (2) was checked by restricting the potential range between 0.2 and 0.8 V. Unfortunately, the Mg_3Sb_2 electrode exhibited very poor cycle life performance (see in Fig. 8). If the lithium-insertion reaction proceeded based on the formation of LiMgSb and Li_3Sb corresponding to Eqs. (2) and (3), the theoretical capacity was estimated to ca. $510\,mA\,h\,g^{-1}$. The observed capacity was much larger than the theoretical one. The formation of solid electrolyte interface (SEI) layer and/or the oxidation of lithium by oxygen dissolved in the alloy would be used to explain the excessive charge capacity at the first charge. On the other hand, the large irreversible capacity at the first cycle indicates that a large amount of lithium was stabilized in the electrode. In the case of the non-graphitizable (hard) carbon electrode, many lithium ions could be inserted into defect sites. The MA-method would introduce high density defect sites into Mg_3Sb_2, so that the inserted lithium appears to be trapped at the defect sites and hardly extracted in the discharge process.

To improve the cycle life performance of Mg_3Sb_2 electrode, we tried to mechanically push lithium as a third element into the Mg–Sb alloy. Fig. 6 shows XRD patterns of the mechanically alloyed products using magnesium, antimony and lithium as starting materials. A typical cubic phase appeared with a tiny antimony peak after mechanical alloying for 20 h. The lattice parameter of the cubic phase was calculated to be $a = 661.9\,pm$ which coincided with that of LiMgSb (MgAgAs-type structure) [31].

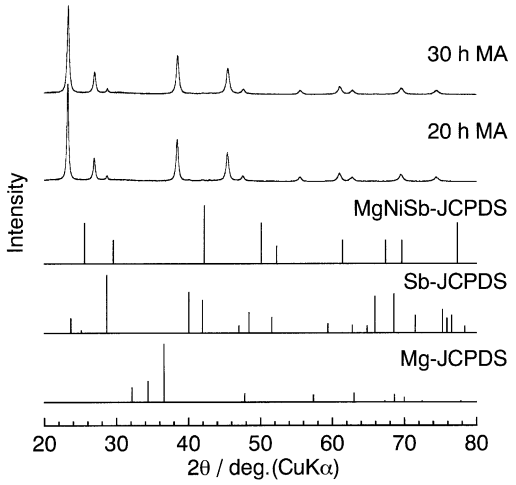

Fig. 6. XRD patterns of the mechanical alloyed Li–Mg–Sb mixture. The JCPDS data of MgNiSb with the MgAgAs-type structure was listed under a reference.

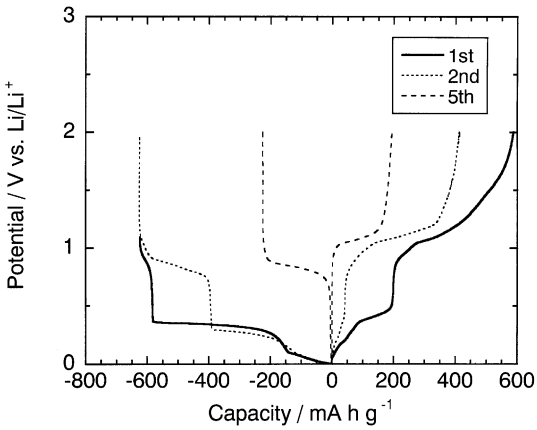

Fig. 7. Charge–discharge curves for the electrode of LiMgSb synthesized by mechanical alloying.

The potential profiles of the Li/LiMgSb cell are shown in Fig. 7. Surprisingly, a coulombic efficiency of LiMgSb electrode was estimated to close to 100% at the first cycle; no irreversible capacity was observed. Besides, the LiMgSb electrode exhibited the same change in the potential plateaus as Mg_3Sb_2 electrode. These facts appear to indicate that the electrode reaction of LiMgSb is dominated by alloying–dealloying of Li_3Sb corresponding to Eq. (3). Cycle life performances of the Mg_3Sb_2 and LiMgSb electrodes are shown in Fig. 8. In the first few cycles, the LiMgSb electrode exhibited a sharp decline as well as the Mg_3Sb_2 one. However, the discharge efficiency of the LiMgSb electrode is kept at about 100% after the fifth cycle. The poor cycle life performance of the Mg_3Sb_2 electrode would be due to a grain refinement during cycling and subsequently a lack of electrical conductivity. Mechanical addition of lithium as a third element into Mg_3Sb_2 would prevent the grain refinement. In addition, the difference in the cyclability between LiMgSb and Mg_3Sb_2 electrodes may be explained by the difference in morphology between the mechanically and electrochemically lithiated Mg_3Sb_2. In particular, we think that the core of Mg_3Sb_2 particle has

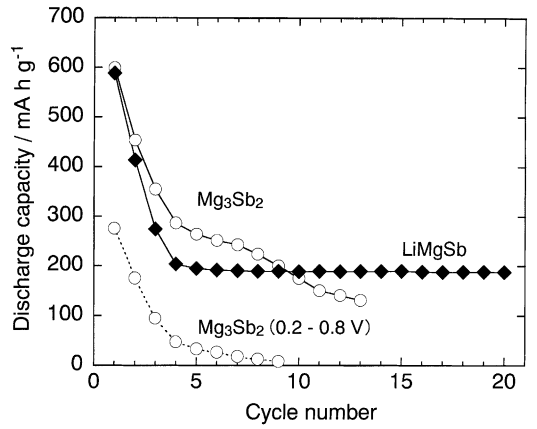

Fig. 8. Cyclability of discharge capacity for the Mg_3Sb_2 and LiMgSb electrodes.

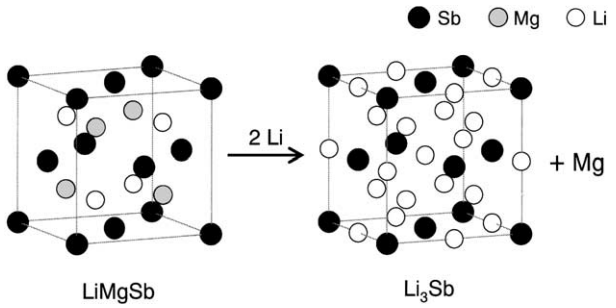

Fig. 9. Schematic drawings for the transition of LiMgSb to Li_3Sb.

not been lithiated yet at the early cycles, although the presence of Mg_3Sb_2 phase was not revealed by XRD patterns at 0 and 0.2 V, as shown in Fig. 4. As for the mechanically lithiated LiMgSb electrodes, the lithium distribution would be uniform in a grain since the first charging. In the first discharging process, the region of the potential plateau was wider at more than 1.0 V for LiMgSb than for Mg_3Sb_2 (see in Figs. 3 and 7). This plateau appears to correspond to the extraction of lithium from Li–Sb alloy. In other words, the LiMgSb electrode is to react with lithium to form Li_3Sb completely, as compared with the Mg_3Sb_2 electrode. Accordingly, the mechanical strain during further charge will be different between these of two electrodes.

The good cyclability of the LiMgSb electrode may be also explained by the crystallographic relationship between LiMgSb and Li_3Sb. The transition of LiMgSb to Li_3Sb, as shown in Fig. 9, can proceed when the inserted lithium is substituted for magnesium in the LiMgSb structure. Lithium can accommodate octahedral site (4b) besides the ordinary magnesium site in LiMgSb. On the other hand, the antimony atoms maintain their spatial positions during the phase change. Using the lattice parameters of LiMgSb and Li_3Sb, $a = 662$ and 657 pm, the phase transition should be accompanied only by a 2% contraction in volume. The intermetallic compounds that could accommodate lithium with relatively small volume change have attraction for practical use. As shown in Fig. 4, there is no striking difference in the XRD patterns between LiMgSb and Li_3Sb phases. Slight peak shift in diffraction angle toward higher angle sides was observed in the charged sample to 0 V, indicating the decrease in the lattice parameter with the formation Li_3Sb. When the potential reached to 1.3 V at discharge process, the position of diffraction peaks returned to the initial position, meaning the reconstruction of LiMgSb. The alike crystallographic property between the structures of charged and discharged electrodes would contribute to the improvement of the cyclability.

4. Conclusions

Mg_3Sb_2 and LiMgSb were synthesized by mechanical alloying. The electrodes made of the alloys were found to

electrochemically absorb and desorb lithium. A gravimetric discharge (lithium extraction) capacity of both these electrodes was ca. 600 mA h g^{-1}. As for the Mg_3Sb_2 electrode, the first volumetric discharge capacity was estimated to be 2400 mA h cm^{-3}. Ex situ XRD results show that Mg_3Sb_2 reacted with lithium to form LiMgSb during the charge process. Further reaction with lithium results in the formation of Li_3Sb at lower voltages, meaning the decomposition of LiMgSb phase. The cyclic voltammograms suggest that the principal lithium-insertion mechanism of Mg_3Sb_2 is based on the formation and decomposition of Li–Sb alloy. Although the cycle life performance of Mg_3Sb_2 electrode was very poor, the cyclability was drastically improved by mechanical adding lithium to Mg_3Sb_2 (the ball-milled LiMgSb electrode). Furthermore, the LiMgSb electrode exhibited no irreversible capacity at the first charge–discharge cycle.

Acknowledgements

This work was supported by a grant-in-aid for Scientific Research from the Ministry of Education, Culture, Sports, Science and Technology, and a grant from the Electric Technology Research Foundation of Chugoku and the Asahi Glass Foundation.

References

[1] A.N. Dey, J. Electrochem. Soc. 118 (1971) 1547.
[2] D. Fauteux, R. Koksbang, J. Appl. Electrochem. 23 (1993) 1.
[3] Y. Idota, T. Kubota, A. Matsufuji, Y. Maekawa, T. Miyasaka, Science 276 (1997) 1395.
[4] J.O. Besenhard, J. Yang, M. Winter, J. Power Sources 68 (1997) 87.
[5] R.A. Huggins, R. Koksbang, J. Power Sources 81–82 (1999) 13.
[6] O. Mao, J.R. Dahn, J. Electrochem. Soc. 146 (1999) 414.
[7] J. Yang, M. Winter, J.O. Besenhard, Solid State Ionics 90 (1996) 281.
[8] J. Yang, Y. Takeda, N. Imanishi, O. Yamamoto, J. Electrochem. Soc. 146 (1999) 4009.
[9] J. Yang, Y. Takeda, N. Imanishi, T. Ichikawa, O. Yamamoto, Solid State Ionics 135 (2000) 175.
[10] K.D. Kepler, J.T. Vaughey, M.M. Thackeray, Electrochem. Solid-State Lett. 2 (1999) 307.
[11] K.D. Kepler, J.T. Vaughey, M.M. Thackeray, J. Power Sources 81–82 (1999) 383.
[12] D. Larcher, L.Y. Beaulieu, D.D. MacNeil, J.R. Dahn, J. Electrochem. Soc. 147 (2000) 1658.
[13] Y. Xia, T. Sakai, T. Fijieda, M. Wada, H. Yoshinaga, Electrochem. Solid-State Lett. 4 (2001) A9.
[14] H. Sakaguchi, H. Honda, T. Esaka, Denki Kagaku (presently Electrochemistry) 66 (1998) 1291.
[15] H. Sakaguchi, H. Honda, T. Esaka, J. Power Sources 81–82 (1999) 224.
[16] H. Sakaguchi, H. Honda, H. Maeta, T. Esaka, Jpn. Inst. Metals Proc. 12 (1999) 1305.
[17] H. Honda, H. Sakaguchi, T. Fukunaga, T. Esaka, Electrochemistry 70 (2002) 99.
[18] H. Kim, J. Choi, H.-J. Sohn, T. Kang, J. Electrochem. Soc. 146 (1999) 4401.
[19] R. Alcantara, F.J. Fernandez-Madrigal, P. Lavela, J.L. Tirado, J.C. Jumas, J.C. Olivier-Fourcade, J. Mater. Chem. 9 (1999) 2517.
[20] H. Sakaguchi, H. Maeta, M. Kubota, H. Honda, T. Esaka, Electrochemistry 68 (2000) 632.
[21] G.S. Cao, X.B. Zhao, T. Li, C.P. Lu, J. Power Sources 94 (2001) 102.
[22] X.B. Zhao, G.S. Cao, C.P. Lv, L.J. Zhang, S.H. Hu, T.J. Zhu, B.C. Zhou, J. Alloys Compd. 315 (2001) 265.
[23] J.T. Vaughey, C.S. Johnson, A.J. Kropf, R. Benedek, M.M. Thackeray, H. Tostmann, T. Sarakonsri, S. Hackney, L. Fransson, K. Edstrõm, J.O. Thomas, J. Power Sources 97–98 (2001) 194.
[24] K.C. Hewitt, L.Y. Beaulieu, J.R. Dahn, J. Electrochem. Soc. 148 (2001) A402.
[25] H. Kim, Y.-J. Kim, D.G. Kim, H.-J. Sohn, T. Kang, Solid State Ionics 144 (2001) 41.
[26] H. Sakaguchi, T. Esaka, HYOMEN (SURFACE in Japanese) 39 (2001) 239.
[27] M.M. Thackeray, J.T. Vaughey, L.M.L. Fransson, JOM 54 (2002) 20.
[28] R.A. Huggins, Solid State Ionics 61–68 (2002) 152.
[29] H. Sakaguchi, H. Honda, Y. Akasaka, T. Esaka, J. Power Sources, in press.
[30] H. Honda, H. Sakaguchi, Y. Fukuda, T. Esaka, Mater. Res. Bull. 38 (2003) 647.
[31] G. Laves, J.D' Ans, E. Lax, FIAT Rev. Ger. Sci. (1948).